Electric Flux Density Learning Method for Solving Three-Dimensional Electromagnetic Scattering Problems

Tiantian Yin, Chao-Fu Wang, Kuiwen Xu, Yulong Zhou, Yu Zhong, Xudong Chen, *Fellow*, *IEEE*

***Abstract*— Inspired by a discretized formulation resulting from volume integral equation and method of moments, we propose an electric flux density learning method (EFDLM) using cascaded neural networks to solve three-dimensional electromagnetic (EM) scattering problems that involve lossless dielectric objects. The inputs of the proposed EFDLM consist of the contrast of the objects, the projections of incident field and the first-order scattered field onto the testing functions, and the output is chosen as the normalized electric flux density. Analyses on the computational complexity, computation time and memory usage of the EFDLM are conducted to fully understand its fundamental features. Numerical simulations clearly show that the proposed method outperforms black-box learning method, which chooses the contrast and incident field as its inputs and the total electric field as its output. It is also demonstrated that the EFDLM is able to solve the scattering problems of dielectric objects with higher contrasts by increasing the number of sub-networks. Further, the pros and cons of the proposed learning approach for solving EM scattering problems are discussed, where some caveats are provided to avoid using learning approaches in a black-box way.**

***Index Terms*—Electromagnetic field, deep learning, volume integral equations**

I. Introduction

Analysis of electromagnetic (EM) scattering from three-dimensional (3D) dielectric objects has been in great demand as a basic necessity of many application areas, such as medical imaging, remote sensing, etc. The commonly-used numerical methods for this kind of problem include finite difference method (FDM) [1], [2], finite element method (FEM) [3] and method of moments (MoM) [3], among others.

Compared to other numerical methods, the MoM avoids numerically truncating an infinite domain to a finite domain due to its use of appropriate Green's function. Note that the truncation process usually requires sophisticated absorbing boundary conditions [4]. To solve the matrix equations formulated by the MoM, iterative methods [5]-[7] are commonly used, which have higher computational efficiency than direct methods such as Gaussian elimination method. Iterative methods could be accelerated using different kinds of fast algorithms. Typical fast algorithms include impedance matrix localization (IML) [8], complex multipole beam approach (CMBA) [9], multilevel matrix decomposition algorithm (MLMDA) [10], adaptive cross approximation (ACA) algorithm [11], multilevel fast multipole algorithm (MLFMA) [12], fast Fourier transform (FFT)-accelerated methods [4], [7], [13], etc. For 3D dielectric scatterers, the FFT-accelerated methods use uniform grids and are easy to implement. To formulate an FFT-accelerated method, integral equation has to be converted to its discretized matrix equation by choosing appropriate basis functions and testing functions. To solve the volume integral equation (VIE) of 3D dielectric scatterers for electric field or electric flux density, pulse basis functions should be avoided since they will produce fictitious charge densities in boundary of cells and lead to inaccurate solutions for high contrast objects [14]. To address this issue, those basis functions that are able to form continuous electric flux density or electric field within homogeneous medium, such as volumetric rooftop functions, should be used [6], [7], [15].

With the development of high-performance computing facilities, deep learning (DL) techniques have been intensively studied and widely applied to solve EM scattering problems [16]. For electrostatic problems, fully-connected neural networks and convolutional neural networks (CNNs) are used to solve the Poisson's equations [17]-[20]. For two-dimensional (2D) dielectric scattering problem of transverse electric (TE) polarization, an improved U-net based method is proposed to solve its magnetic field [21]. For transverse magnetic (TM) polarization, a generative adversarial network is used to calculate the induced current in [22] and cascaded neural networks that employ the residual of discretized electric field integral equation (EFIE) are used to solve for the total electric field in [23], [24]. For modelling electrically large objects, the neural networks have been used to accelerate MLFMA [25]. To model the scattering of TM polarization from 2D conducting objects, combined field integral equation (CFIE), combining the EFIE and magnetic field integral equation (MFIE), has been solved by use of a cascaded neural network [26]. DL techniques have also been applied to predict the scattered field of different structures such as doubly periodic structures [27], nano-structures [28], [29],

Corresponding author: Xudong Chen.

T. Yin, Y. Zhou, X. Chen are with the Department of Electrical and Computer Engineering, National University of Singapore, 117583, Singapore (e-mail: eleyint@nus.edu.sg; e0338289@u.nus.edu; elechenx@nus.edu.sg).

C.-F. Wang is with National University of Singapore, 117411, Singapore (e-mail: cfwang@nus.edu.sg).

K. Xu is with Engineering Research Center of Smart Microsensors and Microsystems, Ministry of Education, Hangzhou Dianzi University, Hangzhou 310018, China (e-mail: kuiwenxu@hdu.edu.cn).

Y. Zhong is with the Institute of High Performance Computing, A*STAR, 138632, Singapore (e-mail: zhongyu@ihpc.a-star.edu.sg).

dielectric metasurfaces [30]. We find that, to obtain satisfying results for scattering problems of dielectric objects, we could either use a powerful neural network or provide more information about wave physics to a neural network.

In this paper, we propose a cascaded neural network, referred to as electric flux density learning method (EFDLM) that is inspired by iterative solvers of EM scattering problems involving 3D lossless dielectric scatterers. To avoid using machine learning in a black-box way, we should fully make use of insightful domain knowledge on wave scattering, which presents well-known mathematical properties (or even analytical formulas) that do not need to be learned by training with a lot of data. Under the general guidelines of how profitably combining DL with the available knowledge on underlying physics of wave scattering, we have carefully looked into the structure of the iterative solver of discretized VIE and proposed the EFDLM. The contributions of this paper are fourfold as follows:

1. The proposed method is based on the discretized VIE that uses the volumetric rooftop functions as both basis functions and testing functions. Note that the normal component of the electric flux density is continuous at boundaries of dielectric objects, whereas the normal component of the electric field is not. Therefore, the discretized VIE is formulated in terms of the electric flux density instead of the electric field [15]. Since the proposed neural network implicitly learns the process of solving the VIE, we choose the electric flux density as the output of the network.
2. The projection of the first order scattered field onto the testing functions is introduced as an additional input of the neural network. Since the first-order scattered field, defined in the Born series of the total electric field, involves the Green's function, the input of the EFDLM has in certain degree involved wave physics inside.
3. EFDLM consists of several sub-networks that are cascaded together, where the residual of the VIE corresponding to the output of the previous sub-network is calculated and subsequently is chosen as the input of the next sub-network. This kind of cascade is motivated by the traditional iterative solver for scattering problems. The residual helps the next sub-network to determine a new searching direction and measures how good the output of the previous sub-network is.
4. By conducting the analyses on the computational complexity, computation time and memory usage of the proposed EFDLM, we discuss the pros and cons of the learning approach for solving EM scattering problems, where some caveats are provided to avoid using learning approach in a black-box way.

The structure of the paper is as follows. In Section II, the formulation of discretized equation of VIE using volumetric rooftop functions as both basis functions and testing functions is provided. The proposed cascaded neural network for solving 3D EM scattering problem is also presented. In Section III, the comparison between the EFDLM and the black-box method, as well as the comparison between EFDLMs using different number of sub-networks is provided. In Section IV, the conclusions and discussions are given.

II. Formulations

A. Three-Dimensional Scattering Problem

For 3D scattering problems of dielectric objects, the VIE [15] is defined as

$$\frac{\mathbf{D}(\mathbf{x})}{\varepsilon(\mathbf{x})} - (k_0^2 + \nabla\nabla\cdot)\mathbf{A}(\mathbf{x}) = \mathbf{E}^{\text{inc}}(\mathbf{x}), \tag{1}$$

where $\mathbf{x} = (x_1, x_2, x_3)$, $\mathbf{D}$ is the electric flux density, $\mathbf{E}^{\text{inc}}$ is the incident electric field, ε is the permittivity, k_0 is the wavenumber of the free space. $\mathbf{A}$ is the vector potential that is given by:

$$\mathbf{A}(\mathbf{x}) = \frac{1}{\varepsilon_0}\int_V G(\mathbf{x}-\mathbf{x}')\beta(\mathbf{x}')\mathbf{D}(\mathbf{x}')d\mathbf{x}', \tag{2}$$

where ε_0 is the permittivity of the free space, the normalized contrast

$$\beta(\mathbf{x}) = \frac{\varepsilon(\mathbf{x}) - \varepsilon_0}{\varepsilon(\mathbf{x})} \tag{3}$$

is related to the well-known contrast $\chi(\mathbf{x})$ by $\beta(\mathbf{x}) = \frac{\varepsilon_0}{\varepsilon(\mathbf{x})}\chi(\mathbf{x})$, and the 3D scalar Green's function is

$$G(\mathbf{x}-\mathbf{x}') = \frac{\exp(ik_0|\mathbf{x}-\mathbf{x}'|)}{4\pi|\mathbf{x}-\mathbf{x}'|}. \tag{4}$$

By applying the testing function $\Psi_{M,M,P}^{(p)}$ to (1), we obtain [5]-[7], [15]:

$$\begin{aligned}\int_{\mathbf{x}\in V}\psi_{M,N,P}^{(p)}(\mathbf{x})E_p^{inc}(\mathbf{x})d\mathbf{x} &= \int_{\mathbf{x}\in V}\psi_{M,N,P}^{(p)}(\mathbf{x})\frac{D_p(\mathbf{x})}{\varepsilon(\mathbf{x})}d\mathbf{x} \\ -k_0^2\int_{\mathbf{x}\in V}\psi_{M,N,P}^{(p)}(\mathbf{x})A_p(\mathbf{x})d\mathbf{x} &+ \int_{\mathbf{x}\in V}\frac{d\psi_{M,N,P}^{(p)}(\mathbf{x})}{dx_p}\nabla\cdot\mathbf{A}(\mathbf{x})d\mathbf{x},\end{aligned} \tag{5}$$

where $p = 1,2,3$ is the index of the three coordinate directions, and $M, N, P \in [1, L]$ are the index of grids for the scattering domain V with dimension $(L-1)\Delta x \times (L-1)\Delta x \times (L-1)\Delta x$. The electric flux density, the vector potential and the incident field are represented by the volumetric rooftop basis functions:

$$D_q(\mathbf{x}) = \varepsilon_0\sum_{I,J,K} d_{I,J,K}^{(q)}\psi_{I,J,K}^{(q)}(\mathbf{x}), \tag{6}$$

$$A_q(\mathbf{x}) = \sum_{I,J,K} A_{I,J,K}^{(q)}\psi_{I,J,K}^{(q)}(\mathbf{x}), \tag{7}$$

$$E_q^{inc}(\mathbf{x}) = \sum_{I,J,K} E_{I,J,K}^{inc,(q)}\psi_{I,J,K}^{(q)}(\mathbf{x}). \tag{8}$$

where $q = 1,2,3$, and $I, J, K \in [1, L]$. After the substitution of (6)- (8), (5) become:

$$\begin{aligned}e_{M,N,P}^{inc,(p)} &= \sum_{I,J,K}\sum_{q=1}^{3} d_{I,J,K}^{(q)}u_{M,N,P;I,J,K}^{(p,q)} \\ &+ A_{I,J,K}^{(q)}\left[-k_0^2 v_{M,N,P;I,J,K}^{(p,q)} + w_{M,N,P;I,J,K}^{(p,q)}\right],\end{aligned} \tag{9}$$

where

$$e_{M,N,P}^{inc,(p)} = \sum_{I,J,K} \sum_{q=1}^{3} E_{I,J,K}^{inc,(q)} v_{M,N,P;I,J,K}^{(p,q)} , \quad (10)$$

$$u_{M,N,P;I,J,K}^{(p,q)} = \delta_{p,q} \int_{\mathbf{x}\in V} \psi_{M,N,P}^{(p)}(\mathbf{x}) \frac{\varepsilon_0}{\varepsilon(\mathbf{x})} \psi_{I,J,K}^{(q)}(\mathbf{x}) d\mathbf{x} , \quad (11)$$

$$v_{M,N,P;I,J,K}^{(p,q)} = \delta_{p,q} \int_{\mathbf{x}\in V} \psi_{M,N,P}^{(p)}(\mathbf{x}) \psi_{I,J,K}^{(q)}(\mathbf{x}) d\mathbf{x} , \quad (12)$$

$$w_{M,N,P;I,J,K}^{(p,q)} = \int_{\mathbf{x}\in V} \frac{d\psi_{M,N,P}^{(p)}(\mathbf{x})}{dx_p} \frac{d\psi_{I,J,K}^{(q)}(\mathbf{x})}{dx_q} d\mathbf{x}, \quad (13)$$

where $\delta_{p,q}$ equals to 1 when $p = q$ and 0 otherwise. The volumetric rooftop basis function for the first coordinate direction is defined as

$$\begin{aligned} \psi_{M,N,P}^{(1)}(\mathbf{x}) = \Lambda(x_1 - x_{1;M,N,P} + \frac{1}{2}\Delta x; 2\Delta x) \\ \cdot\Pi(x_2 - x_{2;M,N,P}; \Delta x) \\ \cdot\Pi(x_3 - x_{3;M,N,P}; \Delta x), \end{aligned} \quad (14)$$

where $\Lambda(x; 2\Delta x)$ is a one-dimensional triangle function centered at x with support $2\Delta x$, $\Pi(x; \Delta x)$ is a one-dimensional pulse function centered at x with support Δx, $\{x_{1;M,N,P}, x_{2;M,N,P}, x_{3;M,N,P}\}$ denotes the coordinates of the centers of the volumetric grids. The volumetric rooftop basis functions for the second and the third coordinate directions are defined in a similar way as in (14) [15].

The coefficients of the vector potential in (9) can be calculated by [15]:

$$A_{I,J,K}^{(q)} = \Delta x^3 \sum_{I',J',K'} G_{I-I',J-J',K-K'} \beta_{I',J',K'}^{(q)} d_{I',J',K'}^{(q)} , \quad (15)$$

where

$$G_{I\text{-}I',J\text{-}J',K\text{-}K'} = [G]\big((I\text{-}I')\Delta x, (J\text{-}J')\Delta x, (K\text{-}K')\Delta x\big), \quad (16)$$

$$[G](x_1, x_2, x_3) = \begin{cases} \dfrac{(1-\frac{1}{2}ik_0\Delta x)\exp(\frac{1}{2}ik_0\Delta x) - 1}{\frac{1}{6}\pi k_0^2 (\Delta x)^3} & \sqrt{x_1^2 + x_2^2 + x_3^2} = 0, \\ \exp(ik_0\sqrt{x_1^2 + x_2^2 + x_3^2}) \cdot & \\ \dfrac{\left[\dfrac{\sinh(\frac{1}{2}ik_0\Delta x)}{\frac{1}{2}ik_0\Delta x} - \cosh(\frac{1}{2}ik_0\Delta x)\right]}{\frac{1}{3}\pi(k_0\Delta x)^2\sqrt{x_1^2 + x_2^2 + x_3^2}} & \sqrt{x_1^2 + x_2^2 + x_3^2} > \frac{1}{2}\Delta x. \end{cases} \quad (17)$$

In the scattering problem, (9) could also be simplified and written as [7]:

$$\mathbf{L}^{\text{opr}}\mathbf{d} = \mathbf{e}^{\text{inc}} , \quad (18)$$

where $\mathbf{e}^{\text{inc}}$, $\mathbf{L}^{\text{opr}}$ are known and $\mathbf{d}$ is unknown. From (6), we understand that $\mathbf{d}$ represents the coefficients of the normalized electric flux density using volumetric rooftop functions as basis functions. On the other hand, $\mathbf{d}$ could also be regarded as the normalized electric flux density at the centers of the basis functions. $\mathbf{e}^{\text{inc}}$ is the projected incident field onto the testing functions and $\mathbf{L}^{\text{opr}}$ contains the information about the contrast and the Green's function. To solve the scattering problem, the normalized electric flux density $\mathbf{d}$ could be calculated using FFT-accelerated iterative methods, such as the transpose-free quasi-minimal residual-FFT (TFQMR-FFT) method [7]. A key step in iterative solver is:

$$\mathbf{d}^{\text{n}} = \mathbf{d}^{\text{n-1}} + \Delta\mathbf{d}, \quad (19)$$

where $\mathbf{d}^{\text{n}}$ is the result at the nth iteration step and $\Delta\mathbf{d}$ can be obtained by solving a least square problem in an approximated way,

$$Min: \left\| \mathbf{L}^{\text{opr}}\Delta\mathbf{d} - (\mathbf{e}^{\text{inc}} - \mathbf{L}^{\text{opr}}\mathbf{d}^{\text{n-1}}) \right\|^2, \quad (20)$$

where $(\mathbf{e}^{\text{inc}} - \mathbf{L}^{\text{opr}}\mathbf{d}^{n-1})$ is defined to be the residual of $\mathbf{d}^{\text{n}-1}$ in (18).

B. EFDLM

1) Inputs, Output and Loss Function

The EFDLM consists of cascaded sub-networks, as shown in Fig. 1(a). Each sub-network is a variant of CNN, or more precisely the U-net. For convenience, we refer to the nth sub-network as CNN_n, which is shown in Fig. 1(c).

Inspired by the formulation in (9) and (18), we propose a cascaded neural network to solve for the normalized electric flux density. The total electric field could be easily calculated from the predicted normalized electric flux density as the ratio of electric flux density in (6) to the permittivity.

It is well-known that the total electric field could be represented using the Born series [31] as

$$\begin{aligned} \mathbf{E}^{\text{t}} = \mathbf{E}^{\text{inc}} + G_d(\frac{\varepsilon - \varepsilon_0}{\varepsilon_0}\mathbf{E}^{\text{inc}}) + G_d(\frac{\varepsilon - \varepsilon_0}{\varepsilon_0} G_d(\frac{\varepsilon - \varepsilon_0}{\varepsilon_0}\mathbf{E}^{\text{inc}})) \\ + G_d(\frac{\varepsilon - \varepsilon_0}{\varepsilon_0} G_d(\frac{\varepsilon - \varepsilon_0}{\varepsilon_0} G_d(\frac{\varepsilon - \varepsilon_0}{\varepsilon_0}\mathbf{E}^{\text{inc}})))..., \end{aligned} \quad (21)$$

where

$$G_d(\mathbf{f})(\mathbf{x}) = (k_0^2 + \nabla\nabla\cdot)\int_V G(\mathbf{x} - \mathbf{x}')\mathbf{f}(\mathbf{x}')d\mathbf{x}' \quad (22)$$

For electrically small and low contrast scatterers, the Born series is convergent. The second term on the right hand side of (21) is the first-order scattered field. Motivated by the Born series, the inputs of the first sub-network of the proposed EFDLM consist of the contrast $\boldsymbol{\chi}$ in (23), the projection of incident field $\mathbf{e}^{\text{inc}}$ in (24) and the projection of first order scattered field $\mathbf{E}^{\text{first}}$ in (25), which are given as:

$$\chi_{M,N,\text{P}} = \frac{\varepsilon_{M,N,P} - \varepsilon_0}{\varepsilon_0} , \quad (23)$$

$$e_{M,N,P}^{inc,(p)} = \sum_{I,J,K} \sum_{q=1}^{3} E_{I,J,K}^{inc,(q)} v_{M,N,P;I,J,K}^{(p,q)} , \quad (24)$$

$$E_{M,N,P}^{\text{first},(p)} = \sum_{I,J,K} \sum_{q=1}^{3} A_{I,J,K}^{0,(q)} \left[k_0^2 v_{M,N,P;I,J,K}^{(p,q)} - w_{M,N,P;I,J,K}^{(p,q)} \right] , \quad (25)$$

where

$$A_{I,J,K}^{0,(q)} = \frac{1}{\varepsilon_0}\Delta x^3 \sum_{I',J',K'} G_{I-I',J-J',K-K'} \beta_{I',J',K'}^{(q)} \varepsilon_{I',J',K'}^{(q)} E_{I',J',K'}^{inc,(q)} . \quad (26)$$

For lossless and isotropic scatterers, the contrast is a real scalar. Therefore, the contrast $\boldsymbol{\chi}$ only needs one input channel.

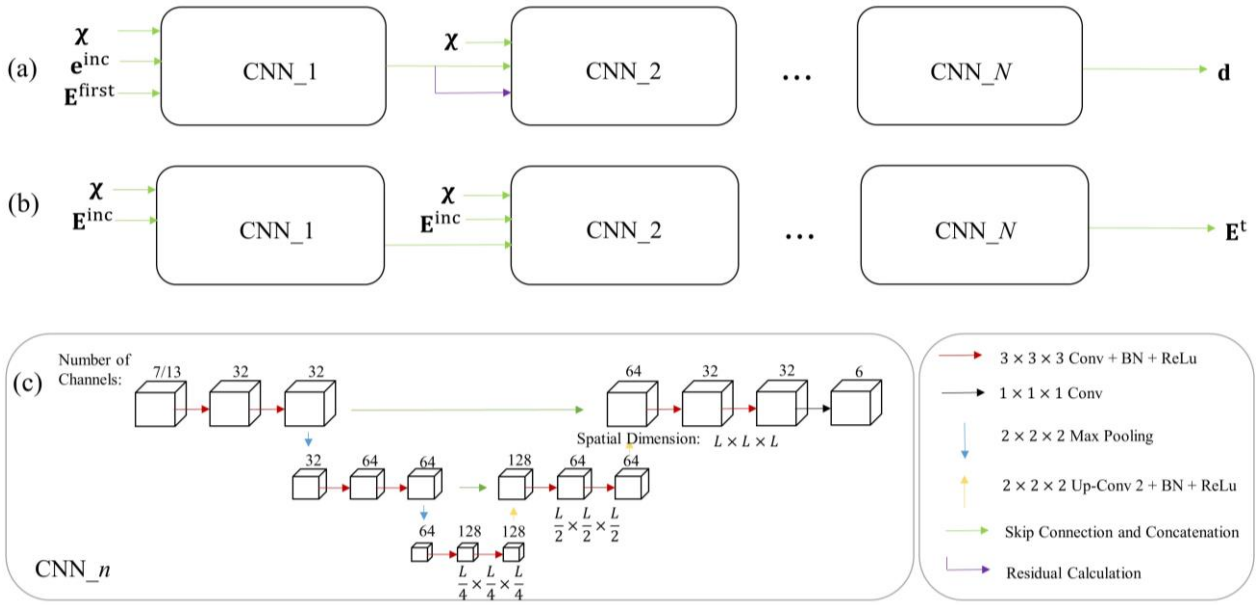

Fig. 1 The neural network structure of (a) EFDLM, (b) black-box method, (c) the structure of sub-network.

TABLE I
AVERAGE COMPUTATION TIME AND MEMORY USAGE FOR DIFFERENT METHODS

Method	Contrast Range	Average Computation Time	Memory Usage
TFQMR-FFT	0.5-1.5	0.90s	16.84 MB
	1.5-2.5	1.80 s	23.88 MB
EFDLM (CNN1+CNN2)	0.5-1.5	0.012 s	11.39 GB, 192.07 MB
EFDLM (CNN1+CNN2+CNN3)	1.5-2.5	0.025 s	24.42 GB, 405.44 MB

The complex-valued $\mathbf{e}^{\text{inc}}$ and $\mathbf{E}^{\text{first}}$ have three directions and each of them needs 6 channels. In total, 13 input channels per grid are used for the first sub-network of EFDLM. Consequently, the size of input is $L \times L \times L \times 13$.

The output of EFDLM is the normalized electric flux density $\mathbf{d}$. Since the complex-valued $\mathbf{d}$ at each grid needs 6 channels, the size of output is equal to $L \times L \times L \times 6$. The loss function of the proposed EFDLM is the mean square error between the outputs of the neural network and the normalized electric flux density that is calculated by the TFQMR-FFT method.

2) Cascade of Sub-Networks

The EFDLM consist of cascaded sub-networks. The way of cascade is motivated by the iteration steps of traditional iterative solver. From (19) and (20), we see that the next-step solution depends on the operator $\mathbf{L}^{\text{opr}}$, the current step solution and its residual. Therefore, for the nth sub-network of EFDLM, the inputs are chosen as the contrast $\boldsymbol{\chi}$, on which $\mathbf{L}^{\text{opr}}$ depends, the output of the previous sub-network $\mathbf{d}^{n-1}$, as well as its residual $\mathbf{R}^{n-1}$ that is defined as:

$$R^{n-1,(p)}_{M,N,P} = e^{inc,(p)}_{M,N,P} - \sum_{I,J,K}\sum_{q=1}^{3} d^{n-1,(q)}_{I,J,K} u^{(p,q)}_{M,N,P;I,J,K} + \sum_{I,J,K}\sum_{q=1}^{3} A^{n-1,(q)}_{I,J,K}\left[k_0^2 v^{(p,q)}_{M,N,P;I,J,K} - w^{(p,q)}_{M,N,P;I,J,K}\right], \quad (27)$$

where

$$A^{n-1,(q)}_{I,J,K} = \Delta x^3 \sum_{I',J',K'} G_{I-I',J-J',K-K'} \beta^{(q)}_{I',J',K'} d^{n-1,(q)}_{I',J',K'}. \quad (28)$$

Hence, the size of input of the subsequent sub-networks is also equal to $L \times L \times L \times 13$.

C. Black-Box Method

For comparison, we briefly introduce a black-box method of using DL. Without considering any physical principles, the black-box method directly uses the incident field and the contrast to predict the total electric field. The black-box method uses a cascaded neural network structure similar to that of EFDLM, as shown in Fig. 1(b). In the black-box method, the size of input of the first sub-network is equal to $L \times L \times L \times 7$ and the size of input of the subsequent sub-networks is equal to $L \times L \times L \times 13$. The size of output of the last sub-network is equal to $L \times L \times L \times 6$. There are three main differences between the black-box method and the proposed method. First, in the black-box method, the incident field and the contrast are used as inputs for the first sub-network without doing any projections. Second, the residuals of the outputs of the sub-networks are not calculated and they are replaced by the incident field. Third, the cascaded neural network of the black-box method directly predicts the total electric field instead of the normalized electric flux density.

D. Computational Complexity, Computation Time, and Memory Usage

The computational complexity of the TFQMR-FFT method

is $O(N_{iter}L^3\log(L^3)))$, where N_{iter} is the total number of iterations. The computational complexity of the proposed EFDLM is dominated by the convolutions and the residual calculation. The computational complexity of the convolutional layer is $O(L_{fm}^3K^3C_{in}C_{out})$ and the that of the residual calculation is $O(L^3\,log(L^3))$. L_{fm} is the size of the output feature map of the layer in one dimension, C_{in} is the number of input channels of the layer, C_{out} is the number of output channels of the layer, K is the kernel size in one dimension.

Using 1200 samples, the calculated average computation time of the TFQMR-FFT method and the EFDLM for one sample is shown in Table I. The stop criterion of the TFQMR-FFT method is $\left\|\mathbf{e}^{\text{inc}}-\mathbf{L}\mathbf{d}^{\text{n}}\right\|_2/\left\|\mathbf{e}^{\text{inc}}\right\|_2 \le 10^{-8}$, where $\|\cdot\|_2$ denotes the L^2 norm. The memory usages of the EFDLM and the TFQMR-FFT method are also shown in Table I. For the EFDLM, the memory usages are different in the training and testing stages. To show the difference, the first value in the Table I represents the memory usage of training and the second one represents the memory usage of testing. Note that the memory usage of training is dependent on the batch size and the optimizer. The results in Table I are calculated by use of the batch size 32 and the Adam optimizer [32]. From Table I, we see that the proposed EFDLM has a much faster computational speed than the TFQMR-FFT method. However, the EFDLM also requires more memories in both training and testing stages than the TFQMR-FFT method.

III. Numerical Results

A. Numerical Setup

In numerical simulations, the operating frequency is 300 MHz. The size of the scattering domain is 1 m × 1 m × 1 m. The training and validation datasets are formed by samples composed of 3 to 6 spheres that are allowed to overlap. The radii of the spheres are randomly distributed between 0.2 m to 0.3 m. Three plane wave incidences are used. The first incident wave propagates in the x direction with a linear polarization in the z direction. The second incident wave propagates in the y direction with a linear polarization in the x direction. The third incident wave propagates in the z direction with a linear polarization in the y direction.

For comparison, the performance of the neural networks is evaluated by the relative error that is defined by:

$$R_e = \sqrt{\sum_{M=1}^{L-1}\sum_{N=1}^{L-1}\sum_{P=1}^{L-1}\sum_{q=1}^{3}\left|E^{(q)}_{predicted;M,N,P;} - E^{(q)}_{true;M,N,P}\right|^2} \Big/ \sqrt{\sum_{M=1}^{L-1}\sum_{N=1}^{L-1}\sum_{P=1}^{L-1}\sum_{q=1}^{3}\left|E^{(q)}_{true;M,N,P}\right|^2}, \quad (29)$$

where $|\cdot|$ denotes the absolute value, $E^{(q)}_{predicted;M,N,P}$ is the predicted total electric field and $E^{(q)}_{true;M,N,P}$ is the total electric field calculated by the TFQMR-FFT method. For multiple testing samples, the relative error is defined as the average of individual relative errors. To effectively display numerical results, for each test, only the contrast profiles in the y-z, x-z and x-y planes are plotted as sub-figures. Among the 3 × 3 sub-figures, the first, second and third rows are the respective plots of y-z, x-z and x-y planes, and the first, second and third columns are the respective plots corresponding to the x, y and z component of electric field. The 3 × 3 sub-figures on the left side of the figures are for the real parts of the results and those on the right side are for the imaginary parts.

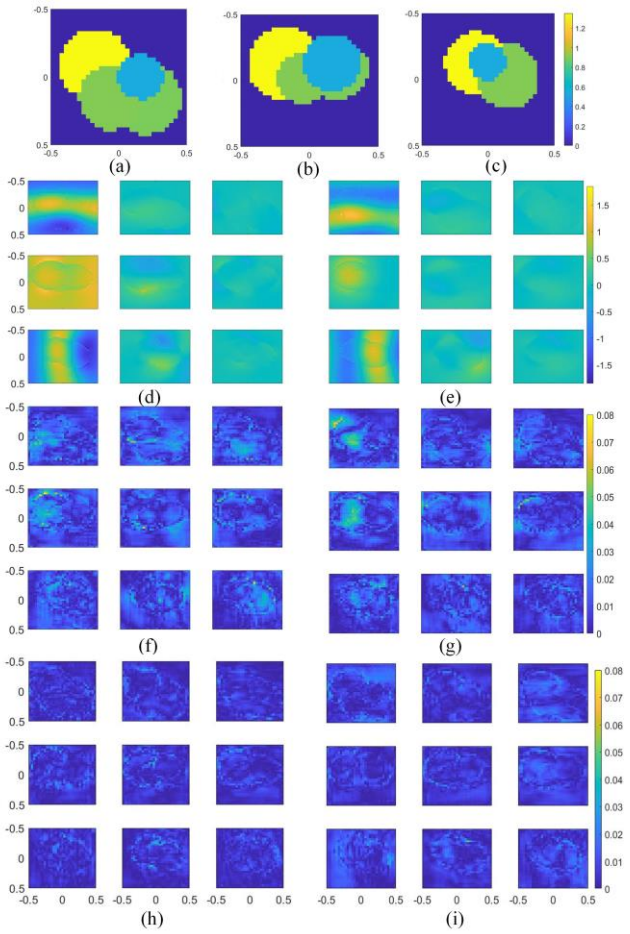

Fig. 2 The sphere example with the contrast between 0.5 and 1.5. The contrast profiles in (a) y-z plane, (b) x-z plane, (c) x-y plane, (d)-(e) the total electric field calculated using the TFQMR-FFT method, (f)-(g) the absolute difference between the predicted field using the black-box method and the true value, (h)-(i) the absolute difference between the predicted field using the EFDLM and the true value. Left and right columns are for the results of real and imaginary parts, respectively.

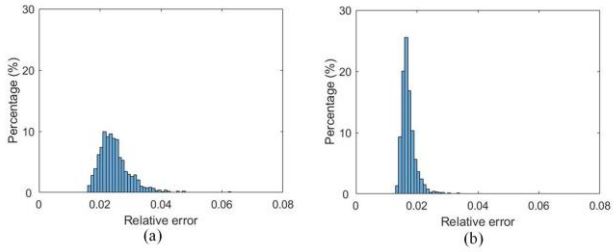

Fig. 3 The histograms of relative errors of the testing samples with contrast between 0.5 and 1.5 using (a) the black-box method, (b) the EFDLM with two sub-networks.

B. Implementation Details

In this paper, all the DL-based methods and iterative method are implemented in Python. The computation platform is a server with one AMD Ryzen Threadripper 3990X 64-Core CPU 2.9 GHz, and one NVIDIA GeForce RTX 3090 GPU.

The Adam optimizer is used for training. The initial learning rate is set to be 10^{-3} and the batch size is equal to 32. The training processes of all the trained neural networks contain 800

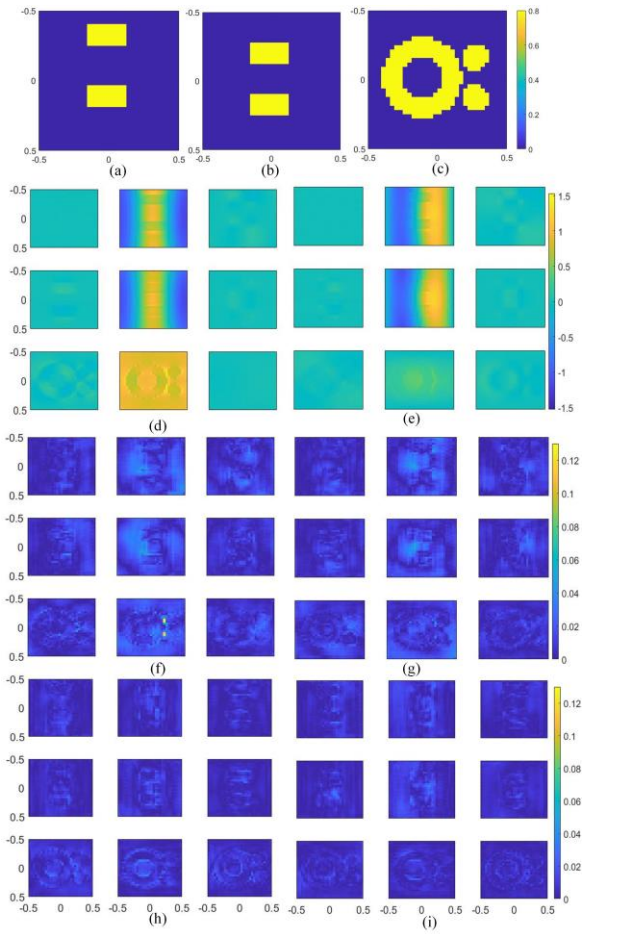

Fig. 4 The "Austria" ring example with the contrast 0.8. The meaning of subfigures (a)-(i) is the same as those of Fig. 2.

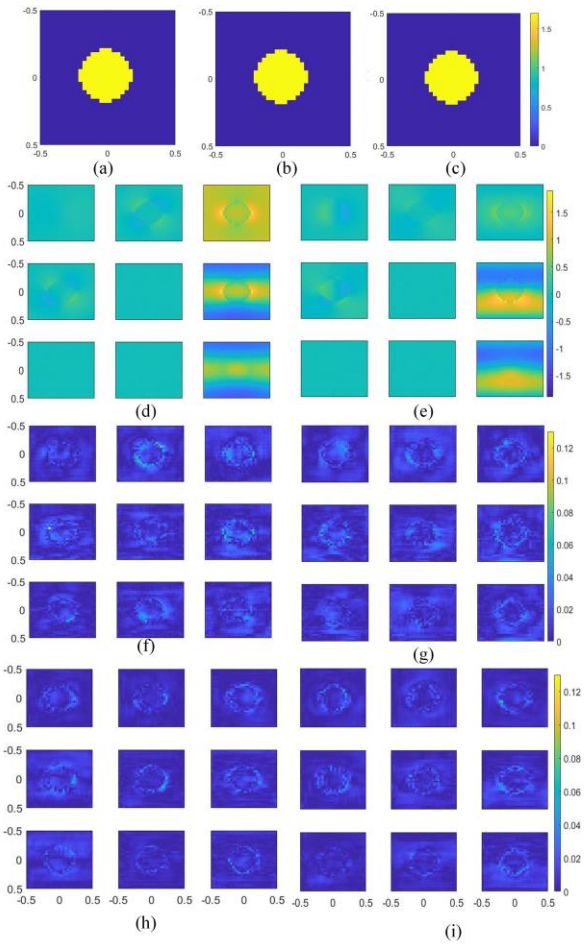

Fig. 5 The sphere example with the contrast 1.7. The meaning of subfigures (a)-(i) is the same as those of Fig. 2.

epochs. For the proposed EFDLM, the total training time using two sub-networks for solving the scattering problems of scatterers with contrast between 0.5 and 1.5 is about 50 hours and that for scatterers with contrast between 1.5 and 2.5 is about 96 hours. Note that, to save the GPU memory, a data generator has been used in the training process to load training data from data files into GPU batch by batch, which leads to much longer training time than loading all the training data into GPU at once.

C. Comparison Between EFDLM and the Black-Box Method

In this section, the EFDLM and the black-box method are trained using the same training dataset and their performances are compared. In the training and validation datasets, the contrast of the spheres is randomly distributed between 0.5 and 1.5. For this range of contrast, we find that it suffices for the EFDLM and the black-box method to use two sub-networks. Considering the wavelength of the fields in both free space and scatterers, the scattering domain is discretized into $31 \times 31 \times 31$ grids. The size of the input $\boldsymbol{\chi}$ is $32 \times 32 \times 32$. The size of the inputs $\mathbf{e}^{\text{inc}}$, $\mathbf{E}^{\text{first}}$ and $\mathbf{E}^{\text{inc}}$ is $32 \times 32 \times 32 \times 6$. The size of the output $\mathbf{d}$ is $32 \times 32 \times 32 \times 6$. The training and the validation datasets contain 3,840 and 960 samples, respectively.

In the first example, the contrasts and the shapes of the testing scatterers are both within the training range. The incident wave propagates in the *y* direction with a linear polarization in the *x* direction. The predicted results using the EFDLM and the black-box method are shown in Fig. 2. It can be observed that the relative error of EFDLM is smaller than the relative error of the black-box method. To quantitatively compare the performance of both methods, 1200 samples are generated. The relative errors of the 1200 samples using both methods are calculated and then the average value is shown in Table II. The relative error using the EFDLM is equal to 1.84% and the relative error using the black-box method is 2.51%. The histograms of the relative errors using both methods are also plotted in Fig. 3. It is observed from Fig. 3 that, for most of the 1200 samples, the relative errors of the EFDLM are smaller than 2%, which is not the case for the black-box method.

In the second example, a scatterer that is out of the training range is tested to evaluate the networks' generalization ability. The cross-section shape of the scatterer in the *x*-*y* plane is an "Austria" ring [33], as shown in Fig. 4(c). The "Austria" ring is formed by two circles with the radius equal to 0.1 m and a ring with the inner radius equal to 0.15 m and the outer radius equal to 0.3 m. The width of the scatterer in the z direction is 0.3 m. The contrast of the scatterer is 0.8. This scatterer can be regarded as four cylinders and is consequently different from the scatterers' shapes in the training dataset. The incident wave propagates in the *z* direction with a linear polarization in the *y* direction. The predicted results are plotted in Fig. 4. The relative errors are 1.66% and 2.68% for the EFDLM and the

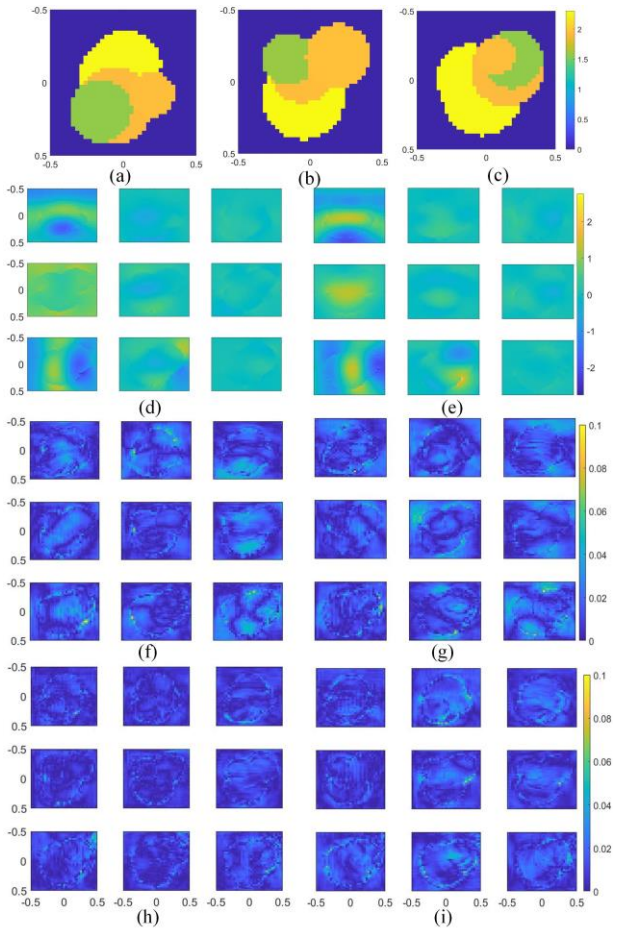

Fig. 6 The sphere example with the contrast between 1.5 and 2.5. The contrast profiles in (a) *y*-*z* plane, (b) *x*-*z* plane, (c) *x*-*y* plane, (d)-(e) the total electric field calculated using the TFQMR-FFT method, (f)-(g) the absolute difference between the predicted field using the EFDLM with two sub-networks and the true value, (h)-(i) the absolute difference between the predicted field using the EFDLM with three sub-networks and the true value.

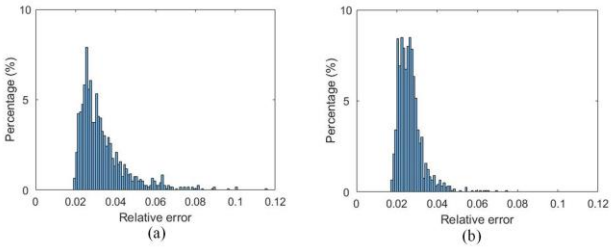

Fig. 7 The histograms of relative errors of the testing samples with contrast between 1.5 and 2.5 using the proposed EFDLM with (a) two sub-networks and (b) three sub-networks.

black-box method, respectively, which shows the advantage of the former over the latter.

In the third example, a sphere scatterer with radius equal to 0.2 m and contrast equal to 1.7 is chosen. The contrast of the scatterer is out of the training range. The incident wave propagates in the *x* direction with a linear polarization in the *z* direction. It can be seen from Fig. 5 that the proposed method can generate satisfying results that are more accurate than the black-box method. The relative errors of the proposed method and the black-box method are 1.75% and 2.35%, respectively.

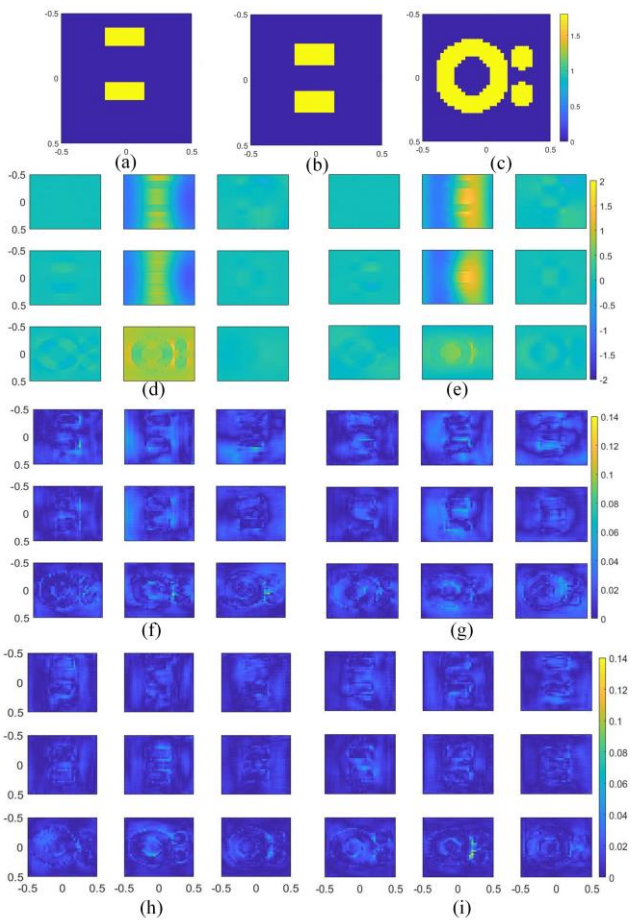

Fig. 8 The "Austria" ring example with the contrast 1.8. The meaning of subfigures (a)-(i) is the same as those of Fig. 6.

D. Comparison of EFDLM Using Different Number of Sub-Networks for Higher Contrast Scatterers

In this section, the performances of EFDLM using two sub-networks and three sub-networks are compared for the cases of higher contrast scatterers. In the training and validation datasets, the contrast of spheres is randomly distributed between 1.5 and 2.5. A finer discretization is needed and the scattering domain is discretized into $35 \times 35 \times 35$ grids. The size of the input $\boldsymbol{\chi}$ is $36 \times 36 \times 36$. The sizes of the inputs $\mathbf{e}^{\mathrm{inc}}$, $\mathbf{E}^{\mathrm{inc}}$ and $\mathbf{E}^{\mathrm{first}}$ are all equal to $36 \times 36 \times 36 \times 6$. The size of the output $\mathbf{d}$ is $36 \times 36 \times 36 \times 6$. The training and the validation datasets contain 5,760 and 1,440 samples, respectively.

In the first example, the contrasts and the shapes of scatterers are within the training range. The incident wave propagates in the *y* direction with a linear polarization in the *x* direction. The predicted results for the scatterer that is shown in Fig. 6(a)-(c) are plotted in Fig. 6(f)-(i). It is apparent that the EFDLM using three sub-networks has better predicted results than the EFDLM using two sub-networks. The relative errors of 1200 test samples are calculated. The average relative errors using two sub-networks and three sub-networks are 3.34% and 2.67%, respectively, as shown in Table III. As the EFLDM with three sub-networks is deeper with more tunable parameters, it is reasonable that it has better performance than the neural network with two sub-networks. The histograms of relative

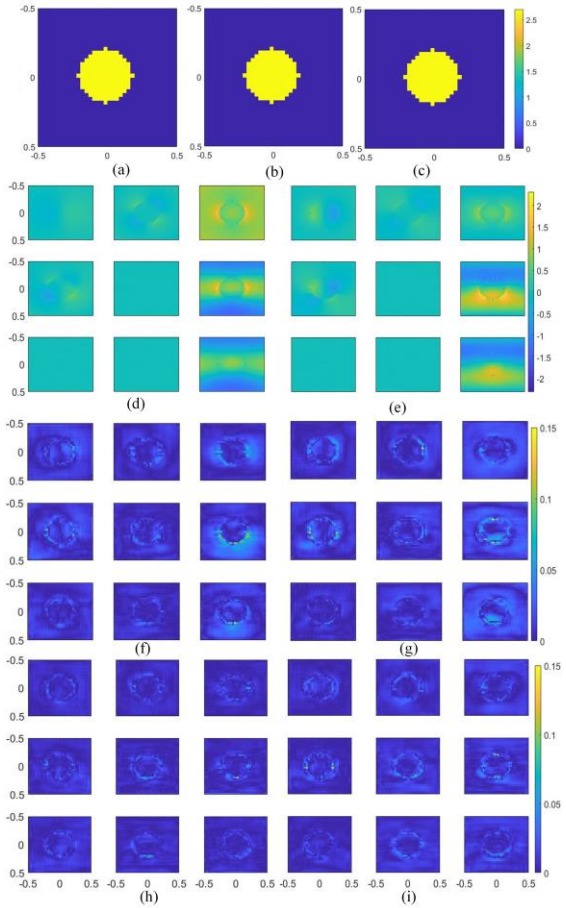

Fig. 9 The sphere example with the contrast 2.7. The meaning of subfigures (a)-(i) is the same as those of Fig. 6.

TABLE II
THE RELATIVE ERRORS FOR BLACK-BOX METHOD AND EFDLM WITH 2 SUB-NETWORKS THAT ARE TRAINED USING TRAINING SAMPLES WITH CONTRAST BETWEEN 0.5 AND 1.5

	Black-box	EFDLM (2 sub-networks)
1200 Spheres Samples ($\chi \in [0.5, 1.5]$)	2.51%	1.84%
3D "Austria" Ring ($\chi = 0.8$)	2.68%	1.66%
Sphere ($\chi = 1.7$)	2.35%	1.75%

TABLE III
THE RELATIVE ERRORS FOR EFDLMS WITH 2 SUB-NETWORKS AND 3 SUB-NETWORKS THAT ARE TRAINED USING TRAINING SAMPLES WITH CONTRAST BETWEEN 1.5 AND 2.5

	EFDLM (2 sub-networks)	EFDLM (3 sub-networks)
1200 Spheres Samples ($\chi \in [1.5, 2.5]$)	3.34%	2.67%
3D "Austria" Ring ($\chi = 1.8$)	3.77%	2.46%
Sphere ($\chi = 2.7$)	3.15%	2.00%

errors using different number of sub-networks are plotted in Fig. 7.

In the second example, the "Austria" ring that is reported in Section III C is adopted as a test example, except that the contrast is changed to 1.8. Note that the shape of the scatterer is different from the training dataset, whereas the value of the contrast is in the range of the training dataset. The predictions using both EFDLM with three sub-networks and two sub-networks are plotted in Fig. 8. The relative errors using the EFDLM with three and two sub-networks are 2.46% and 3.77%, respectively. The performances of EFDLM are similar for both the 1200 spheres samples and this "Austria" ring.

In the third example, the testing scatterer has the same shape and incidence as the third example in Section III C, but the contrast is 2.7 that is out of the training range. The predicted results are plotted in Fig. 9. The relative errors of the EFDLM with three sub-networks and two sub-networks are equal to 2.00% and 3.15%, respectively. Although the contrast of the scatterer is out of the training range, the performance of the proposed EFLDM is still satisfying and the performance is better when three sub-networks are used.

IV. CONCLUSIONS AND DISCUSSIONS

In this paper, a learning method based on the discretized VIE is proposed to solve the scattering problems of 3D dielectric objects. The proposed EFDLM implicitly learns the process of solving the VIE by iterative solvers. The proposed EFDLM predicts the normalized electric flux density, and then the total electric field can be easily obtained. The proposed EFDLM makes use of the knowledge on wave physics by introducing the residual calculation and the projection of the first-order scattered field into the neural network. Based on numerical simulation results, together with the analyses on the computational complexity, computation time and memory usage, we provide our opinions on following three items, which could be useful for researchers to solve computational electromagnetics (CEM) problems via learning approaches.

First, we observe that the EFDLM outperforms the black-box method, no matter testing scatterers are in or out of the range of training dataset. The advantage of the proposed EFDLM benefits from the residual calculations of the sub-networks' outputs and the projection of the first-order scattered field. The residual helps the next sub-network to determine a new searching direction and also measures how good the output of the previous sub-network is. The projection of the first-order scattered field contains the information about the Green's function. Note that, although the proposed EFDLM requires convolutions with the Dyadic Green's function, the matrix-vector product could be calculated using the FFT method, which reduces the computational complexity from $O(L^6)$ to $O(L^3 \log(L^3))$.

Second, we discuss the pros and cons of general learning approach for solving EM scattering problems involving dielectric scatterers, compared with traditional non-learning solvers.

1. The mapping functions of neural networks are nonlinear since the output, no matter it is the total electric field or the electric flux density, nonlinearly depends on the variable contrast that is a part of the input. In comparison, traditional non-learning solvers deal with a linear relationship between the total electric field and the incident field for each given scatterer.
2. The mathematical analysis on traditional non-learning solvers, such as accuracy and convergence rate, have been well established. In comparison, the structures of

neural networks, such as the number of layers and the number of neurons per layer, are decided empirically.

3. The adaptability of learning approaches is weak to some extent. For example, if a chosen network is found to be always underfitting during the training process, then we need to improve the network's representation ability by increasing the number of layers and/or the number of neurons per layer. Then, the new network has to be retrained, not being able to use the training results of the previous network. In comparison, if a traditional iterative solver does not converge after a certain number of iterations, then we may simply wait for a few more iterations to reach desired accuracy.
4. Learning approaches have to survive the important challenge of generalization, i.e. when a test case is out of the training range, whereas traditional non-learning solvers do not.
5. Trained neural networks have much faster computational speed, however at the cost of more memory, compared to traditional non-learning solvers.
6. Considering the abovementioned points, learning approaches do not present self-evident advantages if only a small number of scattering problems are solved. Instead, if a larger number of small or medium-scale scattering problems are to be solved, then learning approaches exhibit their advantages, for example, in inverse scattering problems and inverse designs.

Third, we find that it is difficult and computationally expensive for end-to-end learning techniques to train neural networks especially when dealing with the scattering problems of high contrast and/or electrically large size objects. Neural networks accept input such as the contrast and the incident field from one end, and produces output such as the total electric filed or the electric flux density at the other end. End-to-end learning optimizes the network weights by considering the inputs and outputs directly as a whole. On the one hand, for high-contrast or multiscale scattering problems, neural networks may not be able to work properly as VIE based FFT methods converge slowly or not converge. In this case, the preconditioners [34] or domain decomposition method [35] may need to be used together with neural works to solve the scattering problems. On the other hand, more memory, training data, and training time are required for neural networks to solve scattering problems with higher contrast. Our numerical simulations show that while 2-sub-network EFDLM works well for scatterers with contrast between 0.5 and 1.5, its performance decreases for scatterers with contrast between 1.5 and 2.5. For the range between 1.5 and 2.5, 3-sub-network EFDLM has to be adopted to achieve desired accuracy at the cost of significantly increased memory. For a computational domain of $1\,\lambda \times 1\,\lambda \times 1\,\lambda$, the memory for the training of 3-sub-network EFDLM is as large as 24.42 GB that is shown in Table 1. If the contrasts of scatterers are further increased or the electrical size of the scattering domain is enlarged, then it is apparent that much more memory is required and it may need parallel computations using multiple GPUs. The reasons why higher contrast requires more memory, training data and training time are summarized as follows:

1. Neural networks in fact describe the mathematical relationship that maps the input to the output. When contrast is increased, a finer discretization of the scattering domain will be needed since the wavelength inside scatterers is shrunk. Thus, the sizes of both input and output are increased. In addition, the output of network, i.e., total electric field or electric flux density, spatially oscillates faster in scatterer than in background air. Since scatterers can be distributed in any grids within the computational domain, the multi-scale spatial distribution of total electric field or electric flux density is hardly to be sparse due to the randomness of scatterers. To conclude, the sizes of both input and output are increased, which are basically not sparse, for increased contrast, and consequently the mapping between them is more complex and requires neural networks with stronger representation ability by using more layers and/or neurons.
2. Consider a scatterer with the range of contrast $[\chi_{min}, \chi_{max}]$, it is important to note that the range of contrast of the input of neural network is not $[\chi_{min}, \chi_{max}]$, since the input consists of discretized grids occupied by not only scattterers but also air. Thus, the range of the contrast of the input of neural network is $[0, \chi_{max}]$. From the viewpoint of function fitting, a function with a wider range is usually more difficult to be approximated by other functions. For example, a Taylor expansion with linear or quadratic terms might approximate a function well if the range of variables is small, whereas more terms are needed if the range of variables is increased. To conclude, a scatterer with a large value of contrast leads to a larger range of contrast of the input of network, which makes the mapping between the input and the output more complex and requires neural networks with stronger representation ability.
3. Considering the abovementioned two points, if the contrast of scatterer is increased, end-to-end neural networks that are adopted to solve the scattering problem in principle describe a mapping where more output elements collectively depend on more input elements that span wider contrast ranges. Thus, neural networks should be deep enough to approximately represent the rather complex mapping. In addition, sufficient training data are required to capture the main feature of the abovementioned mapping. Note that the ground truth of such a mapping is the physical law of wave scattering, represented by (18). It is apparent that higher contrast requires more memory, training data, and training time.

To conclude, compared to traditional non-learning solvers, learning approaches exhibit their advantages mainly for the cases where a large number of small or medium-scale scattering problems are to be solved, for example, inverse scattering problems and inverse designs. For scatterers with high contrasts, it is difficult and computationally expensive for end-to-end learning techniques to learn the mapping that describes the physical law of scattering. Instead, a more feasible way of solving scattering problems with high contrast is to apply traditional non-learning method as the main solver, which is assisted by neural networks that learn some operators of traditional solvers, such as the gradient and the translation

procedure of MLFMA. This topic will be our next-step research work, i.e., developing hybrid algorithms that adopt the state-of-the-art methods in CEM as the main solver and deploy neural networks to learn some of their operators. Another future research topic is to test the performance of neural networks for lossy dielectric scatterers.

REFERENCE

[1] K. Yee, "Numerical solution of initial boundary value problems involving maxwell's equations in isotropic media," *IEEE Trans. Antennas Propag.*, vol. 14, no. 3, pp. 302-307, 1966.

[2] K. Beilenhoff, W. Heinrich, and H. L. Hartnagel, "Improved finite-difference formulation in frequency domain for three-dimensional scattering problems," *IEEE Trans. Microw. Theory Tech.*, vol. 40, no. 3, pp. 540-546, 1992.

[3] J.-M. Jin, *The finite element method in electromagnetics*. John Wiley & Sons, 2015.

[4] J.-M. Jin, *Theory and computation of electromagnetic fields*. Hoboken, NJ: John Wiley & Sons, 2011.

[5] A. P. M. Zwamborn, P. M. van den Berg, J. Mooibroek, and F. T. Koenis, "Computation of three-dimensional electromagnetic-field distributions in a human body using the weak form of the cgfft method," *ACES J.*, vol. 7, no. 2, pp. 26-42, 1992.

[6] H. Gan and W. C. Chew, "A discrete bcg-fft algorithm for solving 3d inhomogeneous scatterer problems," *J. Electromagn. Waves Appl.*, vol. 9, no. 10, pp. 1339-1357, 1995.

[7] C. Wang and J. Jin, "Simple and efficient computation of electromagnetic fields in arbitrarily shaped inhomogeneous dielectric bodies using transpose-free qmr and fft," *IEEE Trans. Microw. Theory Tech.*, vol. 46, no. 5, pp. 553-558, 1998.

[8] F. X. Canning, "Solution of impedance matrix localization form of moment method problems in five iterations," *Radio Sci.*, vol. 30, no. 5, pp. 1371-1384, 1995.

[9] A. Boag and R. Mittra, "Complex multipole beam approach to electromagnetic scattering problems," *IEEE Trans. Antennas Propag.*, vol. 42, no. 3, pp. 366-372, 1994.

[10] E. Michielssen and A. Boag, "A multilevel matrix decomposition algorithm for analyzing scattering from large structures," *IEEE Trans. Antennas Propag.*, vol. 44, no. 8, pp. 1086-1093, 1996.

[11] A. Schröder, H.-D. Brüns, and C. Schuster, "Fast evaluation of electromagnetic fields using a parallelized adaptive cross approximation," *IEEE Trans. Antennas Propag.*, vol. 62, no. 5, pp. 2818-2822, 2014.

[12] J. Song, C.-C. Lu, and W. C. Chew, "Multilevel fast multipole algorithm for electromagnetic scattering by large complex objects," *IEEE Trans. Antennas Propag.*, vol. 45, no. 10, pp. 1488-1493, 1997.

[13] T. Sarkar, E. Arvas, and S. Rao, "Application of fft and the conjugate gradient method for the solution of electromagnetic radiation from electrically large and small conducting bodies," *IEEE Trans. Antennas Propag.*, vol. 34, no. 5, pp. 635-640, 1986.

[14] A. F. Peterson, S. L. Ray, and R. Mittra, *Computational methods for electromagnetics*. New York: IEEE press, 1998.

[15] P. Zwamborn and P. M. van den Berg, "The three dimensional weak form of the conjugate gradient fft method for solving scattering problems," *IEEE Trans. Microw. Theory Tech.*, vol. 40, no. 9, pp. 1757-1766, 1992.

[16] A. Massa, D. Marcantonio, X. Chen, M. Li, and M. Salucci, "Dnns as applied to electromagnetics, antennas, and propagation—a review," *IEEE Antennas Wireless Propag. Lett.*, vol. 18, no. 11, pp. 2225-2229, 2019.

[17] T. Shan, W. Tang, X. Dang, M. Li, F. Yang, S. Xu, and J. Wu, "Study on a poisson's equation solver based on deep learning technique," *arXiv preprint arXiv:1712.05559*, 2017.

[18] T. Shan, X. Dang, M. Li, F. Yang, S. Xu, and J. Wu, "Study on a 3d possion's equation slover based on deep learning technique," in *2018 IEEE International Conference on Computational Electromagnetics (ICCEM)*, 2018: IEEE, pp. 1-3.

[19] T. Shan, W. Tang, X. Dang, M. Li, F. Yang, S. Xu, and J. Wu, "Study on a fast solver for poisson's equation based on deep learning technique," *IEEE Trans. Antennas Propag.*, vol. 68, no. 9, pp. 6725-6733, 2020.

[20] S. Bhardwaj, H. Gohel, and S. Namuduri, "A multiple-input deep neural network architecture for solution of one-dimensional poisson equation," *IEEE Antennas Wireless Propag. Lett.*, vol. 18, no. 11, pp. 2244-2248, 2019.

[21] S. Qi, Y. Wang, Y. Li, X. Wu, Q. Ren, and Y. Ren, "Two-dimensional electromagnetic solver based on deep learning technique," *IEEE J. Multiscale Multiphys. Comput. Tech.*, vol. 5, pp. 83-88, 2020.

[22] Z. Ma, K. Xu, R. Song, C.-F. Wang, and X. Chen, "Learning-based fast electromagnetic scattering solver through generative adversarial network," *IEEE Trans. Antennas Propag.*, vol. 69, no. 4, pp. 2194-2208, 2021.

[23] R. Guo, T. Shan, X. Song, M. Li, F. Yang, S. Xu, and A. Abubakar, "Physics embedded deep neural network for solving volume integral equation: 2d case," *IEEE Trans. Antennas Propag.*, 2021.

[24] T. Shan, X. Song, R. Guo, M. Li, F. Yang, and S. Xu, "Physics-informed supervised residual learning for 2d electromagnetic forward modeling," *arXiv preprint arXiv:2104.13231*, 2021.

[25] J.-J. Sun, S. Sun, Y. P. Chen, L. Jiang, and J. Hu, "Machine-learning-based hybrid method for the multilevel fast multipole algorithm," *IEEE Antennas Wireless Propag. Lett.*, vol. 19, no. 12, pp. 2177-2181, 2020.

[26] R. Guo, Z. Lin, T. Shan, M. Li, F. Yang, S. Xu, and A. Abubakar, "Solving combined field integral equation with deep neural network for 2d conducting object," *IEEE Antennas Wireless Propag. Lett.*, vol. 20, no. 4, pp. 538 - 542, 2021.

[27] Y. Mao, Q. Zhan, R. Zhang, D. Wang, W.-F. Huang, and Q. H. Liu, "Fast simulation of electromagnetic fields in doubly periodic structures with a deep fully convolutional network," *IEEE Trans. Antennas Propag.*, vol. 69, no. 5, pp. 2921-2928, 2020.

[28] Y. Li *et al.*, "Predicting scattering from complex nano-structures via deep learning," *IEEE Access*, vol. 8, pp. 139983-139993, 2020.

[29] P. R. Wiecha and O. L. Muskens, "Deep learning meets nanophotonics: A generalized accurate predictor for near fields and far fields of arbitrary 3d nanostructures," *Nano Lett.*, vol. 20, no. 1, pp. 329-338, 2019.

[30] M. V. Zhelyeznyakov, S. L. Brunton, and A. Majumdar, "Deep learning to accelerate maxwell's equations for inverse design of dielectric metasurfaces," *arXiv preprint arXiv:2008.10632*, 2020.

[31] R. Kleinman, G. Roach, and P. Van den Berg, "Convergent born series for large refractive indices," *JOSA A*, vol. 7, no. 5, pp. 890-897, 1990.

[32] D. P. Kingma and J. Ba, "Adam: A method for stochastic optimization," *arXiv preprint arXiv:1412.6980*, 2014.

[33] X. Chen, *Computational methods for electromagnetic inverse scattering*. Singapore: Wiley, 2018.

[34] J. Lee, J. Zhang, and C.-C. Lu, "Incomplete lu preconditioning for large scale dense complex linear systems from electromagnetic wave scattering problems," *J. Comput. Phys.*, vol. 185, no. 1, pp. 158-175, 2003.

[35] M. Jiang, J. Hu, M. Tian, R. Zhao, X. Wei, and Z. Nie, "Solving scattering by multilayer dielectric objects using jmcfie-ddm-mlfma," *IEEE Antennas Wireless Propag. Lett.*, vol. 13, pp. 1132-1135, 2014.